

Influence of Argon/oxygen Ratio on Linear and Nonlinear Optical Properties of Copper Doped ZnO Films

Xing WEN¹, Yue HAN¹, Cheng-Bao YAO^{1*}, Ke-Xin ZHANG¹, Jin LI², Wen-Jun SUN¹

¹ Key Laboratory of Photonic and Electric Bandgap Materials, Ministry of Education, School of Physics and Electronic Engineering, Harbin Normal University, Harbin, 150025, China

² College of Information Science and Engineering, Northeastern University, Shenyang, 110819, China

crossref <http://dx.doi.org/10.5755/j01.ms.26.2.21568>

Received 04 September 2018; accepted 16 November 2018

Copper (Cu)-doped ZnO (CZO) films were grown by simultaneous direct current and radio frequency magnetron sputtering technique under the situation of different gas flow rates of Ar: O₂ (1:1, 2:1 and 1:0). The X-ray diffraction patterns revealed the naturally polycrystalline ZnO films with the predominant reflection (002) peak, which referred to the hexagonal wurtzite structure toward c-axis. The elemental composition of thin films was analyzed by energy dispersive spectroscopy (EDS). The Cu concentrations in thin films increased with Ar ratio of up to 1:0. The EDS spectra of three kinds of elements indicate that Cu-doping has obvious and sophisticated effect on the chemical state of oxygen, but less effect on those of copper and zinc. Furthermore, the nonlinear absorption of CZO films was investigated by the way of Z-scan technique. These films demonstrated good nonlinear absorption behavior for the different gas flow rates of Ar: O₂.

Keywords: nonlinear optics, ZnO, thin films.

1. INTRODUCTION

Zinc oxide is one of the most interesting II–VI semiconductors. It is highly transparent, inexpensive, non-toxic, which paves its application way as an active luminescent material, gas sensing and piezoelectric transducers etc [1–5]. To significantly enhance the physical properties of pure Zinc oxide films, all kinds of transition metals [6–10], such as Bi, Ag, Cu, Co and Ni, have been used as dopants at desired doping concentrations using several deposition techniques. Copper is a prominent luminescence activator in II–VI compounds, meanwhile, it changes the luminescence behavior of ZnO through produce a localized impurity levels in the bands structure [11, 12]. Due to the similar ionic radius and electronic shell structure have many physical and chemical properties, which are equivalent to those of Zn [13]. Up to now, multiple solutions have been performed to fabricate the Cu-doped ZnO (CZO) films and explore their excellent applications in optoelectronics by a variety of deposition techniques [14, 15], which include pulsed laser deposition, simultaneous radio frequency (RF) and direct current (DC) magnetron sputtering (MS) and so on. Recent papers have reported on microstructure and different properties of CZO materials, such as electrical, piezooptical effects, optical and photosensitivity properties et al. Structural and optical properties of ZnO films with heavy Cu-doping prepared by MS which were reported by Y. Liu et al. [16]. B. Allabergenov et al. [17] reported microstructural analysis and optical characteristics of CZO films. K. Joshi et al. [18] reported band gap widening and narrowing in CZO films. Taking into account the high deposition rate of simultaneous RF and DC MS technique, through independent doping dopant element to the main body in the crystal lattice, film

is compact and uniform, the structure and optical properties of controllability. In this paper, we research the effect of argon/oxygen ratio on the structural of CZO films. The nonlinear (NL) optical characteristics of CZO films are investigated. The two-photon absorption (TPA) coefficients of CZO films at argon/oxygen ratio are determined.

2. MATERIALS AND EXPERIMENT

Through RF MS ZnO target (99.99 % purity) and DC MS Cu target (99.99 % purity), with different Ar:O₂ (1:1, 2:1 and 1:0) flow rates CZO films were on quartz substrates. The substrates were ultrasonically cleaned by alcohol and deionized water. During the deposition, the base pressure and RF power in the sputtering chamber were 6.0×10^{-4} Pa and 100 W, respectively. The film growth was performed in a growth environment with a ratio of Ar (sputter gas): O₂ (reaction gas) = 20:10 sccm at a constant working pressure of 1.0 Pa.

Many characterization techniques were used to investigate the properties of CZO films. The elemental composition of the CZO films was identified by energy dispersive spectroscopy (EDS, Quanta 200F) attached to the scanning electron microscope (SEM, Quanta 200F). Structural properties have been examined by X-ray diffraction (XRD, D/max-2600/PC). The transmission and absorption spectra were observed at a particular wavelength the extent of 330 to 800 nm using UV–vis spectrophotometer. The NL optical characteristics were studied using nanosecond Z-scan technique, a Q-switched, frequency doubled Nd:YAG (1064 nm) laser producing 532 nm wavelength were used as the excitation source.

* Corresponding author. Tel.: +86-0451-88060525; fax: +86-0451-88060525. E-mail address: yaochengbao5@163.com (C.B. Yao)

3. RESULTS AND DISCUSSION

3.1. Elemental composition

The Cu atomic concentration in the prepared films has been verified by EDS analysis. Fig. 1 a manifest the EDS spectrum for gas flow rates of Ar: O₂ = 1:1. It is confirmed that the deposited films were relation to characteristic Zn and O elements as major intense peaks. Meanwhile, the small peaks of Cu indicated minor composition of Cu²⁺, Cu⁺ has substituted the Zn²⁺ sites in the ZnO host matrix. Fig. 1 b and Fig. 1 c manifest the EDS spectrum for gas flow rates of Ar: O₂ = 2:1 and Ar: O₂ = 1:0, respectively. According to the experimental phenomenon, it is noticed that the reactive gas without oxygen will directly affect the transparency of ZnO films. For example, the gas flow rates of Ar: O₂ = 1:0 resulted in the low transparency films. However, the higher ratio of the oxygen in the reactive gas will not always provide a better transparency.

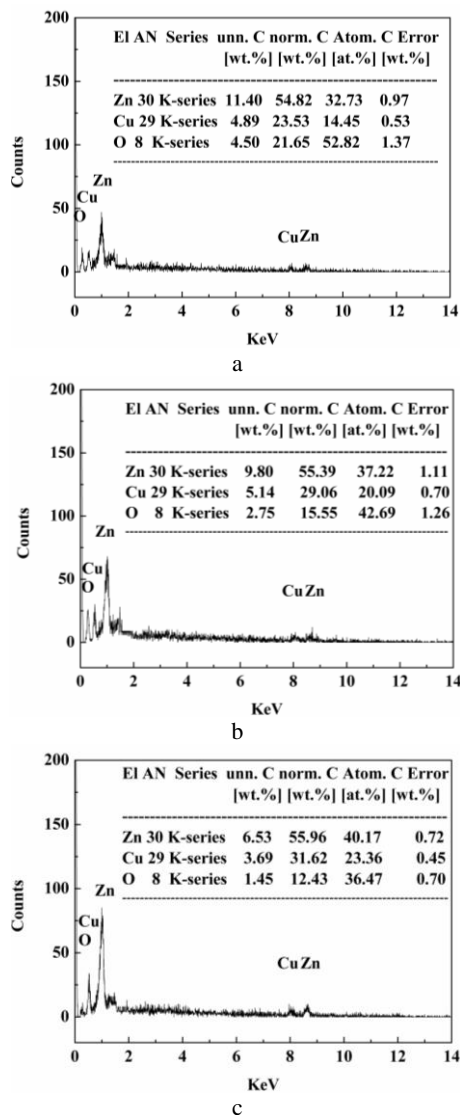


Fig. 1. EDS spectra of CZO films at: Ar:O₂ =: a-1:1; b-2:1; c-1:0

3.2. Surface features

In order to further characterize the effects of gas flow rates on the microstructural properties of the film, SEM

analysis was confirmed, as shown in Fig. 2. All films show the smooth surface without cracks. From the inset (i) of Fig. 2, it can be observed that is size distribution diagram of CZO films for each sample. The average diameter of low-dimensional structure nanocrystal for all the samples were approximately 36 nm (for 1:1), 38 nm (for 2:1), and 40 nm (for 1:0), respectively, referring to the error value of ± 0.14 nm. The particle size is varying from 28 to 48 nm for different gas flow rates. Maximum grain size of 48 nm happened at gas flow rates of Ar: O₂ = 1:0. In Fig. 2, the particle size linearly increases with the Ar ratio. However, it was smaller than Ar ratio of 1:0 compared to the one with the gas flow rates of Ar: O₂ = 2:1. When the Ar ratio increased till to 2:1, there is degradation in particle size because of Cu dopant tends to create more nucleation centers during deposition process. From SEM images, the structure of deposited films can be controlled by adjusting the gas flow rates.

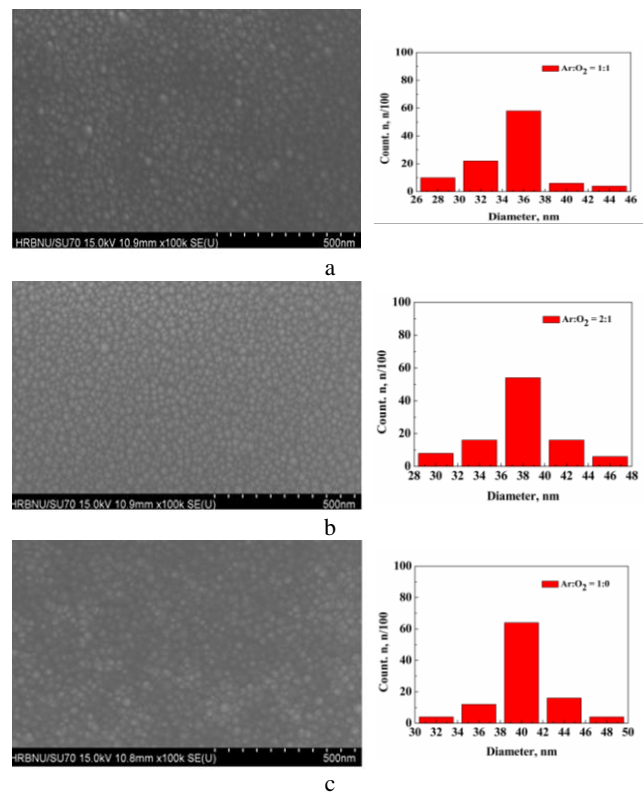


Fig. 2. SEM image of the CZO films at: Ar:O₂ =: a-1:1; b-2:1; c-1:0

3.3. Structural analysis

Fig. 3 shows the XRD patterns of CZO films prepared with simultaneous RF and DC MS technique. From Fig. 3, the crystal particles are arranged closely and the diffraction intensity of the (002) peak. In addition, CZO films at gas flow rates Ar:O₂ (2:1) show the peak intensity with the maximum value. With increasing the gas flow rate, as the interplanar spacing ' d ' ($\lambda = 2d\sin\theta$) increases and the lattice position is replaced by ions of higher ionic radius (ion radius is Cu⁺ ~ 0.077 nm, Zn²⁺ ~ 0.074 nm), the (002) peak position of the zinc oxide structure moves to a lower angle position. The lattice parameters ' a ' and ' c ' values of films can be calculated as [19]

$$a = \lambda / \sqrt{3} \sin \theta_{hkl}; \quad (1)$$

$$c = \lambda / \sin \theta_{hkl}. \quad (2)$$

As shown in Eq. 3, the average crystallite size (D_{hkl}) of the film was assessed by Debye Scherer equation [20, 21].

$$D_{hkl} = k\lambda / \beta \cos \theta_{hkl}, \quad (3)$$

where, the X-ray wavelength is represented by λ , the Bragg diffraction angle is represented by θ_{hkl} , and the full width at half-maximum (FWHM) is represented by β . The lattice parameters and crystallites size of CZO films will increased under different gas flow rates. Nevertheless, the copper composition does not change the hexagonal structure of ZnO films. The (002) diffraction peaks, lattice parameters and average crystallite sizes values estimated for the sample show in Table 1.

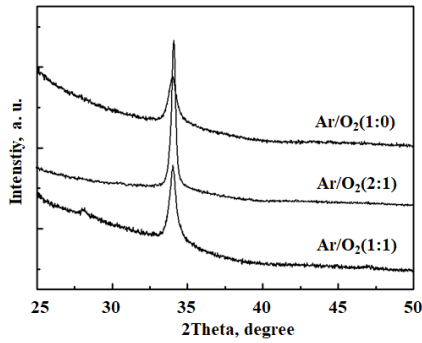


Fig. 3. XRD patterns of CZO films prepared under different gas flow rates

Table 1. The (002) diffraction peaks, lattice parameters and average crystallite size of CZO films under different gas flow rates

Sample	$2\theta, ^\circ$	a, nm	c, nm	D_{hkl} , nm
CZO 1:1	34.41°	0.3296	0.4236	36.23
CZO 1:0	34.14°	0.3292	0.4224	38.12
CZO 2:1	34.20°	0.3286	0.4198	40.34

3.4. X-ray photoelectron spectroscopy analysis

XPS spectra of the CZO film at Ar: O₂ = 1:0 were measured to analyze the valence state of Cu in ZnO film. Fig. 4 shows XPS spectra of the Zn-2p, Cu-2p, and O-1s core level regions of the Cu-ZnO structures. A doublet at 1021.8 eV and 1044.9 eV is observed in Fig. 4 b corresponding to the Zn 2p_{3/2} and 2p_{1/2} core levels. The Cu-2p XPS binding energy region is shown in Fig. 4 c. Photoelectron peaks corresponding to the Cu 2p_{3/2} and 2p_{1/2} core levels were observed at 933.4 eV and 953.7 eV. In handbook of XPS [21], 2p_{3/2} peaks of Cu⁰ and Cu⁺ in Cu₂O appear at the same energy, around 932.7 eV, and that of Cu²⁺ in CuO appears at about 933.6-934 eV. In our experiment, we found that the Cu 2p_{3/2} peak of CZO film at Ar: O₂ = 1:0 had major Cu⁰/Cu⁺ (932.7 eV) and minor (933.8 eV) components. Therefore, it is concluded that Cu ions exist in a mixed oxidation state of +1 and +2 and are predominantly in a univalent and bivalent state in CZO film grown in oxygen poor and enriched environment,

respectively. The conclusion is also consistent with the analysis of XRD results above.

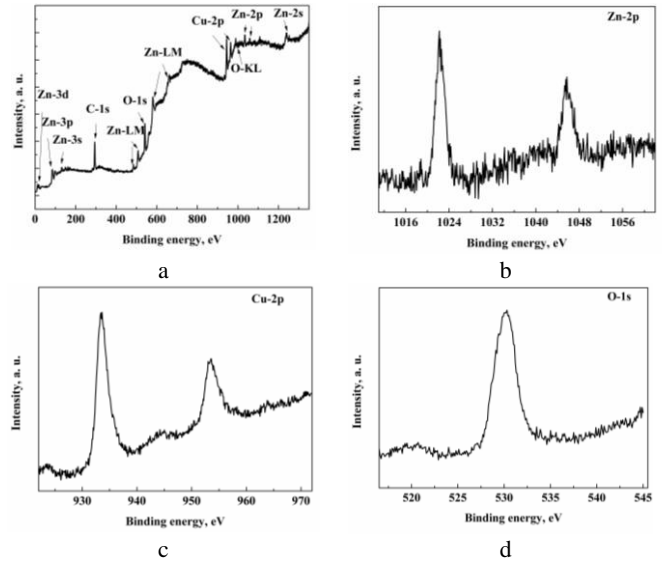


Fig. 4. a–XPS spectra (Al K = 1486.6 eV) corresponding to the CZO films; b–Zn-2p; c–Cu-2p; d–O-1s core level of CZO films

3.5. Linear optical properties

Fig. 5 shows the linear optical absorption and transmission spectrum of the CZO films.

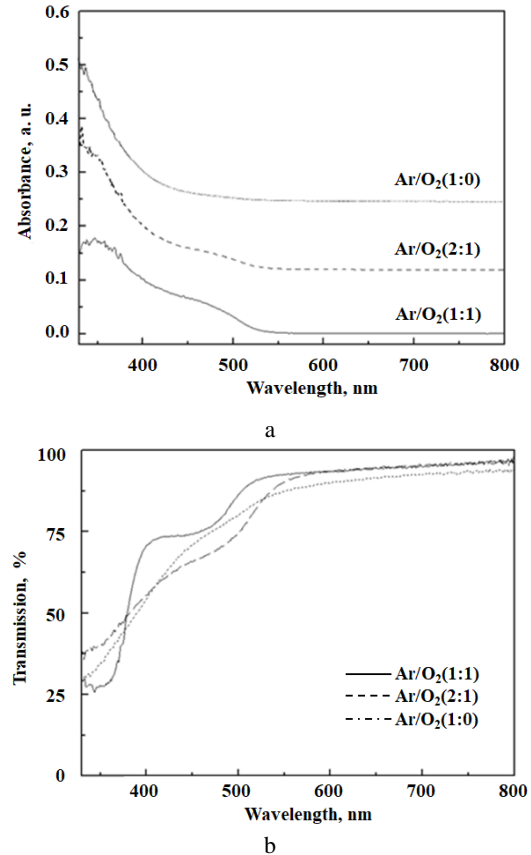


Fig. 5. The absorption (a) and transmission (b) spectra of CZO films formed under different gas flow rates

In Fig. 5 a, the absorption edge conforming to the intrinsic direct band gap in the near UV scope can be

obviously observed. In the wavelength range of 330–800 nm the transmittances were increased with Ar ratio till to 2:1. Notably, the optical transmittance values turn down the following 85 % while using only Ar reactive gas during thin film deposition. This result reveals the gas flow rates affect the transparency of the films. The optical transmittance decreases due to the surface scattering or interstitial positions of the ZnO host lattice, as well as the presence of lattice defects in the ZnO host lattice. In the cause of confirm the direct E_P of ZnO films, we apply the Tauc relationship mentioned in [22–24]. On the basis of the measured absorption spectra, $(ahv)^2$ versus $h\nu$ data of ZnO films with adjust gas flow rates are shown in Fig. 6. It apparently indexes that when copper dopants were introduced, the width of the E_P will broaden with the increase of Ar: O₂ ratio. The E_P values of 3.13, 3.14 and 3.27 eV were obtained at the different gas flow rates of Ar: O₂ = 1:1, 1:0 and 2:1, respectively. We obtained a considerable depression in the E_P energy with gas flow rates. The phenomenon can be ascribed to tough mismatch in the electronegativity of Cu and Zn atoms in ZnO [25, 26].

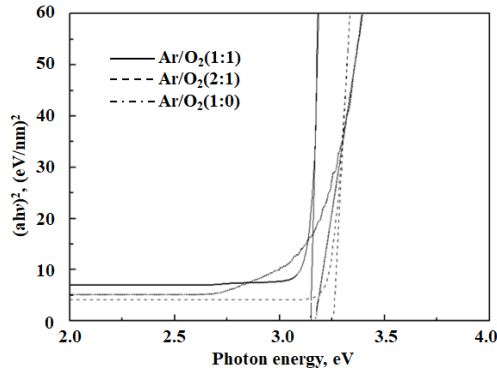


Fig. 6. $(ahv)^2$ versus $(h\nu)$ data of CZO films under different gas flow rates

3.6. Nonlinear optical properties

Fig. 7 manifests normalized open-aperture Z-scan data of CZO films with different gas flow rates (Intensity of laser $I_0 = 120 \text{ MW/cm}^2$ and wavelength $\lambda_{\text{exc}} = 532 \text{ nm}$). As shown in Fig. 7, the transmittance curve exhibits the valley characteristic shape. The normalized transmittance for the standard open aperture Z-scan is expressed by the relationship [27]:

$$T(z, s = 1) = \sum \left([-q_0]^m / (m + 1)^{3/2} \right), \quad (4)$$

where $|q_0(0)| < 1$, $q_0(z) = \alpha_2 I_0 L_{\text{eff}} / (1 + z/z_0)$ (Z_0 : the Rayleigh rang), and the effective length $L_{\text{eff}} = |1 - \exp[-(n-1)\alpha_0 L]| / [(n-1)\alpha_0]$ (α_0 : the linear absorption coefficient and L : the sample thickness).

The value of α_2 was calculated by fitting experimental data to Eq. 4. The results prove that the values of the α_2 were $92.6 \text{ cm}^2/\text{GW}$ (1:1), $98.9 \text{ cm}^2/\text{GW}$ (2:1) and $98.3 \text{ cm}^2/\text{GW}$ (1:0), respectively. So the E_P (3.26 eV or 380 nm) is bigger than two photon energy (1.55 eV), the absorption process of the 532 nm is a TPA process. The results show that all samples performed TPA for laser radiation at 532 nm.

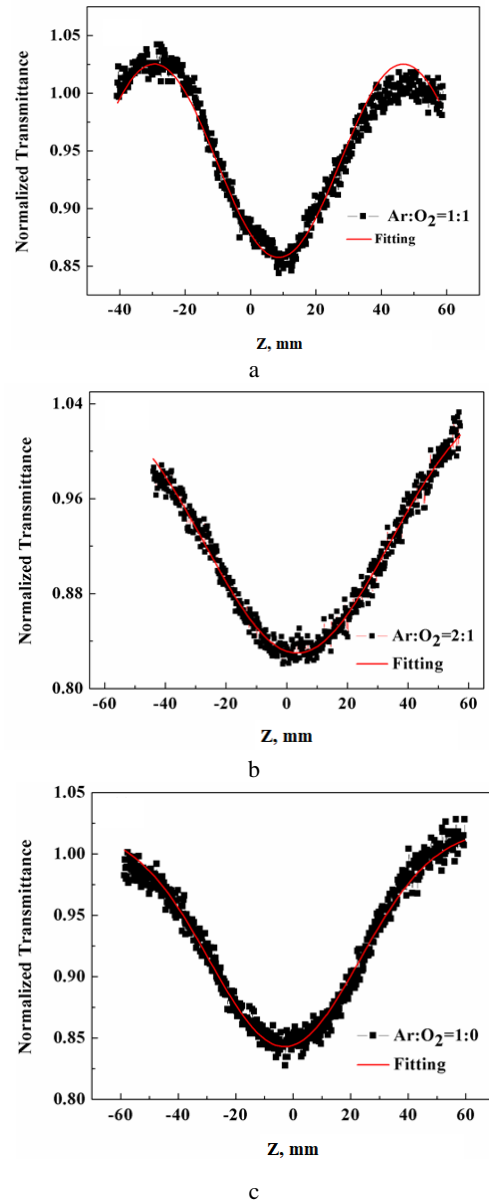


Fig. 7. Normalized open-aperture Z-scan transmittance data of CZO films with different gas rates of Ar:O₂ at 532nm

4. CONCLUSIONS

We synthesized CZO films via magnetron sputtering at various gas flow rates Ar: O₂ (1:1, 2:1 and 1:0) successfully. All CZO films generated in c-axis oriented hexagonal wurtzite crystal structure with ZnO (002) as a mainly reflection. It was found that as gas flow rates increases, while ZnO (002) peak strength will be destroyed by Cu²⁺, Cu⁺ ions instead of Zn²⁺ ion sites. All samples performed the TPA for laser radiation at 532 nm. The values of the TPA coefficient were $92.6 \text{ cm}^2/\text{GW}$ (1:1), $98.9 \text{ cm}^2/\text{GW}$ (2:1) and $98.3 \text{ cm}^2/\text{GW}$ (1:0), respectively. Our studies reveal that these samples have better nonlinear properties with potential applications in optical devices.

Acknowledgements

The National Natural Science Foundation of China (No. 11504072). University Nursing Program for Young

REFERENCES

1. **Hu, J., Gordon, R.G.** Textured Aluminum-Doped Zinc Oxide Thin Films from Atmospheric Pressure Chemical-Vapor Deposition *Journal of Applied Physics* 71 (2) 1992: pp. 880–890.
<https://doi.org/10.1063/1.351309>
2. **Martinez, O., Plaza, J.L., Mass, J., Capote, B., Dieguez, E., Jimenez, J.** Luminescence of Pure and Doped ZnO Films Synthesised by Thermal Annealing on GaSb Single Crystals *Superlattices and Microstructure* 42 (1–6) 2007: pp. 145–151.
<https://doi.org/10.1016/j.spmi.2007.04.024>
3. **Lupan, O., Pauporte, T., Bahers, T.L., Viana, B., Ciofini, I.** Wavelength-Emission Tuning of ZnO Nanowire-Based Light-Emitting Diodes by Cu Doping: Experimental and Computational Insights *Advanced Functional Materials* 21 (18) 2011: pp. 3564–3572.
<https://doi.org/10.1002/adfm.201100258>
4. **Hussain, B., Ebong, A., Ferguson, I.** Zinc Oxide as an Active N-Layer and Antireflection Coating for Silicon Based Heterojunction Solar Cell *Solar Energy Materials and Solar Cells* 139 2015: pp. 95–100.
<https://doi.org/10.1016/j.solmat.2015.03.017>
5. **Li, Y., Gong, J., Deng, Y.** Hierarchical Structured ZnO Nanorods on ZnO Nanofibers and Their Photoresponse to UV and Visible Lights *Sensors and Actuators A: Physical* 158 (2) 2010: pp. 176–182.
<https://doi.org/10.1016/j.sna.2009.12.030>
6. **Hassanien, A.S., Akl, A.A., Saaedi, A.H.** Synthesis, Crystallography, Microstructure, Crystal Defects, and Morphology of Bi_xZn_{1-x}O Nanoparticles Prepared by Sol-Gel Technique *CrystEngComm* 20 2018: pp. 1716–1730.
<https://doi.org/10.1039/C7CE02173A>
7. **Sahu, D.R.** Studies on the Properties of Sputter-Deposited Ag-Doped ZnO Films *Microelectronics Journal* 38 (12) 2007: pp. 1252–1256.
<https://doi.org/10.1016/j.mejo.2007.09.025>
8. **Tarwal, N.L., Gurav, K.V., Mujawar, S.H., Sadale, S.B., Nam, K.W., Bae, W.R., Moholkar, A.V., Kim, J.H., Patil, P.S., Jang, J.H.** Photoluminescence and Photoelectrochemical Properties of the Spray Deposited Copper Doped Zinc Oxide Thin Films *Ceramics International* 40 (6) 2014: pp. 7669–7677.
<https://doi.org/10.1016/j.ceramint.2013.12.108>
9. **Benramache, S., Temam, H.B., Arif, A., Guettaf, A., Belahssen, O.** Correlation between the Structural and Optical Properties of Co Doped ZnO Thin Films Prepared at Different Film Thickness *Optik* 125 (7) 2014: pp. 1816–1820.
<https://doi.org/10.1016/j.ijleo.2013.09.024>
10. **Siddheswaran, R., Savkova, J., Medlin, R., Ocenaseka, J., Zivotsky, O., Novak, P., Sutta, P.** Highly C-Axis Oriented ZnO:Ni Thin Film Nanostructure by RF Magnetron Sputtering: Structural, Morphological and Magnetic Studies *Applied Surface Science* 316 (1) 2014: pp. 524–531.
<https://doi.org/10.1016/j.apsusc.2014.08.068>
11. **Akl, A.A., Mahmoud, S.A., AL-Shomar, S.M., Hassanien, A.S.** Improving Microstructural Properties and Minimizing Crystal Imperfections of Nanocrystalline Cu₂O Thin Films of Different Solution Molarities for Solar Cell Applications *Materials Science in Semiconductor Processing* 74 2018: pp. 183–192.
<https://doi.org/10.1016/j.mssp.2017.10.007>
12. **Tao, Y.M., Ma, S.Y., Chen, H.X., Meng, J.X., Hou, L.L., Jia, Y.F., Shang, X.R.** Effect of the Oxygen Partial Pressure on the Microstructure and Optical Properties of ZnO: Cu Films *Vacuum* 85 (7) 2011: pp. 744–748.
<https://doi.org/10.1016/j.vacuum.2010.11.009>
13. **Bahsi, Z.B., Oral, A.Y.** Effects of Mn and Cu Doping on the Microstructures and Optical Properties of Sol-Gel Derived ZnO Thin Films *Optical Materials* 29 (6) 2007: pp. 672–678.
<https://doi.org/10.1016/j.optmat.2005.11.016>
14. **Jeon, J.H., Jeong, S.Y., Cho, C.R., Lee, S.A., Lee, W.J., Ahn, H.S., Kim, H.S.** Heteroepitaxial Relation and Optical Properties of Cu-Doped ZnO Films Grown by Using Pulsed Laser Deposition *Journal-Korean Physical Society* 54 (92) 2009: pp. 858–862.
<https://doi.org/10.3938/jkps.54.858>
15. **Sahu, D.R.** Properties of Doped ZnO Thin Films Grown by Simultaneous DC and RF Magnetron Sputtering *Materials Science and Engineering: B* 171 (1–3) 2010: pp. 99–103.
<https://doi.org/10.1016/j.mseb.2010.03.080>
16. **Liu, Y., Liu, H.N., Yu, Y., Wang, Q., Li, Y.L., Wang, Z.** Structural and Optical Properties of ZnO Thin Films with Heavy Cu-Doping Prepared by Magnetron Co-Sputtering *Materials Letters* 143 2015: pp. 319–321.
<https://doi.org/10.1016/j.matlet.2014.12.133>
17. **Allabergenov, B., Tursunkulov, O., Abidov, A.I., Byeongdae, C., Wook, J.S., Kim, S.** Microstructural Analysis and Optical Characteristics of Cu-Doped ZnO Thin Films Prepared by DC Magnetron Sputtering *Journal of Crystal Growth* 401 2014: pp. 573–576.
<https://doi.org/10.1016/j.jcrysgro.2014.01.040>
18. **Joshi, K., Rawat, M., Gautam, S.K., Singh, R.G., Ramola, R.C., Singh, F.** Band gap Widening and Narrowing in Cu-Doped ZnO Thin Films *Journal of Alloys and Compounds* 680 2016: pp. 252–258.
<https://doi.org/10.1016/j.jallcom.2016.04.093>
19. **Purohit, A., Chander, S., Sharma, A., Nehra, S.P., Dhaka, M.S.** Impact of Low Temperature Annealing on Structural, Optical, Electrical and Morphological Properties of ZnO Thin Films Grown by RF Sputtering for Photovoltaic Applications *Optical Materials* 49 2015: pp. 51–58.
<https://doi.org/10.1016/j.optmat.2015.08.021>
20. **Bhatti, K.P., Chaudhary, S., Pandya, D.K., Kashyap, S.C.** On the Room-Temperature Ferromagnetism in (ZnO)_{0.98}(MnO₂)_{0.02} *Solid State Communications* 136 (7) 2005: pp. 384–388.
<https://doi.org/10.1016/j.ssc.2005.09.002>
21. **Karamat, S., Mahmood, S., Lin, J.J., Pan, Z.Y., Lee, P., Tan, T.L., Springhama, S.V., Ramanujan, R.V.** Structural, Optical and Magnetic Properties of (ZnO)_{1-x}(MnO₂)_x Thin Films Deposited at Room Temperature *Applied Surface Science* 254 (22) 2008: pp. 7285–7289.
<https://doi.org/10.1016/j.apsusc.2008.05.318>
22. **Sun, J.L., Xu, J., Zhu, J.L.** Oxidized Macroscopic-long Cu Nanowire Bundle Photoconductor *Applied Physics Letters* 90 (20) 2007: pp. 201119.
<https://doi.org/10.1063/1.2741131>
23. **Sakellis, I.** Determining the Activation Volumes in ZnO *Journal of Applied Physics* 112 (1) 2012: pp. 034302.
<https://doi.org/10.1063/1.4729486>
24. **Pankove, J.I. Pankove, J.** Optical Process in Semiconductors, Dover, New York, 1971.

25. **Hassanien, A.S., Aly, K.A., Akl, A.A.** Study of Optical Properties of Thermally Evaporated ZnSe Thin Films Annealed at Different Pulsed Laser Powers *Journal of Alloys and Compounds* 685 2016: pp. 733–742.
<https://doi.org/10.1016/j.jallcom.2016.06.180>
26. **Hassanien, A.S.** Studies on Dielectric Properties, Optoelectrical Parameters and Electronic Polarizability of Thermally Evaporated Amorphous Cd₅₀S_{50-x}Se_x Thin Films *Journal of Alloys and Compounds* 671 2016: pp. 566–578.
<https://doi.org/10.1016/j.jallcom.2016.02.126>
27. **Ferhat, M., Zaoui, A., Ahuja, R.** Magnetism and Band Gap Narrowing in Cu-Doped ZnO *Applied Physics Letters* 94 (14) 2009: pp. 142502–142502-3.
<https://doi.org/10.1063/1.3112603>
28. **Feng, X.B., Ang, Y.L., He, J., Beh, C.W.J., Xu, H.R., Chin, W.S., Ji, W.** Three-Photon Absorption in Semiconductor Quantum Dots: Experiment *Optics Express* 16 (10) 2008: pp. 6999.
<https://doi.org/10.1364/OE.16.006999>